

Feedback-limited Accretion: Luminous Signatures from Growing Planets

M. Gárate,^{1,3,5*} J. Cuadra,^{1,3,4} M. Montesinos^{2,1,3}

¹*Instituto de de Astrofísica, Pontificia Universidad Católica de Chile, Santiago, Chile*

²*Departamento de Astronomía, Universidad de Chile, Casilla 36-D, Santiago, Chile*

³*Millennium Nucleus “Protoplanetary Disks”, Santiago, Chile*

⁴*Max-Planck-Institut für extraterrestrische Physik (MPE), D-85748 Garching, Germany*

⁵*University Observatory, Faculty of Physics, Ludwig-Maximilians-Universität München, Scheinerstr. 1, 81679 Munich, Germany*

Accepted XXX. Received YYY; in original form ZZZ

ABSTRACT

Planets form in discs of gas and dust around stars, and keep growing by accretion of disc material while available. Massive planets clear a gap in that protoplanetary disc, but still accrete through spiral wakes. On its way to the planet, the gas will settle on a *circumplanetary* disc around the planet and slowly accrete on to it. The energy of the accreted gas will be released, heating the planet surroundings in a feedback process. For high enough accretion rates the planet should be detectable at infrared wavelengths. We aim to find whether detectable planet luminosities, $\gtrsim 10^{-3} L_{\odot}$, can occur when considering that the planet luminosity is coupled to the accretion, and also to study which other effects has the feedback on the dynamics of the circumplanetary and the gap regions. We model a planet with mass ratio $q = 10^{-3}$, orbiting at 10 AU from a solar mass star, using a modified version of the 2D code FARGO-AD, which includes a prescription for the accretion and feedback luminosity of the planet. We find that the planetary feedback is able to partially deplete the circumplanetary disc, and to reduce the accretion rate onto the planet. However, detectable luminosities of $L_p \gtrsim 10^{-3} L_{\odot}$ are still produced. The feedback also contributes to partially refilling the gap, to heat up the coorbital region, and to perturb the orbital velocity of the gas.

Key words: protoplanetary discs – planet–disc interactions – accretion, accretion discs – hydrodynamics.

1 INTRODUCTION

Protoplanetary discs are made of gas and dust orbiting a young central star. Giant planets like Jupiter form in these discs once a solid core is massive enough to capture the surrounding gas (Pollack et al. 1996), or if the gas itself becomes self-gravitating and fragments into clumps (Boss 1997). Either way, after a massive planet like Jupiter has formed, it will produce perturbations in the protoplanetary disc due to its gravity, which end up opening a gap when the planet torque exceeds the viscous torque (Lin & Papaloizou 1993; Bryden et al. 1999), and forming a circumplanetary disc (CPD) within the Hill radius (Ayliffe & Bate 2009a). These planet–disc interactions define the early evolution of young planets, so understanding them is key to interpret the observational signatures they produce, such as the width of the gaps produced on the gas or dust distribution, the

presence of spiral arms, or perturbations on the velocity field (e.g., Kanagawa 2015; Dong et al. 2015a,b; Perez et al. 2015; Dipierro et al. 2016).

In addition to those mostly gravitational effects, the accretion of gas on to planets provides another kind of planet formation signatures. After a gap has formed, the CPD will keep providing material to the newly formed planet, and its properties will determine the planet accretion rate (Rivier et al. 2012; Szulágyi et al. 2014). As the planet accretes, the gravitational energy of the gas will be released, heating up the circumplanetary region (Klahr & Kley 2006; Montesinos et al. 2015). This accretion feedback process is expected to perturb the protoplanetary disc, and can be the origin of detectable signatures (Montesinos et al. 2015; Zhu 2015). In recent years there have been multiple possible detections of forming planets within protoplanetary discs (e.g., Quanz et al. 2013), even in the $H\alpha$ emission typically associated with accretion processes (Sallum et al. 2015). These detections can be used to constrain the properties of the embedded

* Email: mgarate@usm.lmu.de

planets once their interplay with the accreting gas is understood.

Besides the observable signatures, the accretion of material could also alter the dynamics of the system as the circumplanetary region is heated. The heating by the accretion on to rocky cores has been shown to change the torque exerted on it, slowing and even reversing the inward migration (Benítez-Llambay et al. 2015). For more massive planets formed in a disc fragmentation process, feedback limits their growth and alters their migration (Nayakshin & Cha 2013; Stamatellos 2015), and hinders further fragmentation (Mercer & Stamatellos 2017)¹. On smaller scales, the CPD region can be depleted by the effect of the feedback (Montesinos et al. 2015), and the heating of the CPD can extend its vertical structure, turning it into an envelope (Szulágyi et al. 2016; Szulágyi 2017).

The goal of this work is to study the interaction between the luminosity of the planet and its accretion rate when both variables are coupled. This extends our previous work presented by Montesinos et al. (2015), in which accretion was not taken into account, and the planet luminosity was a free parameter. Specifically we want to study whether the planet heating could actually deplete the CPD and cut down its source of accretion, or if high planet luminosities can be sustained over time. While this effect may be more or less important for different accretion rates, we are especially interested in planet accretion rates around $10^{-9} - 10^{-8} M_{\odot}/\text{yr}$, which correspond to the accretion of 1 Jupiter mass over $10^5 - 10^6 \text{yr}$. These accretion rates are also interesting because they produce detectable signatures in the protoplanetary disc (Montesinos et al. 2015; Zhu 2015). Additionally, we want to check whether the effects of the planet feedback are limited to the CPD, or if the planet heating affects the rest of the protoplanetary disc. A similar study was already conducted by Klahr & Kley (2006). Our approach is simpler, since we are using an energy transport equation instead of the flux-limited diffusion approximation, and we limit ourselves to two dimensions. However, our model gives us the possibility to study a wider parameter space at higher resolutions.

This paper is structured as follows. In section 2 we present our physical model for the disc and the planet accretion. In section 3 we describe the numerical setup and the parameter space explored. In section 4 we present the results regarding the CPD properties and the planet accretion rate, and in section 5 we show the effects of the feedback on the gap structure. Then, in section 6 we discuss the validity of our model and some possible consequences of our results, concluding in section 7.

2 PHYSICAL MODEL

We use the code FARGO-AD (Baruteau & Masset 2008) to simulate a gas disc around a solar mass star, with a planet on a fixed circular orbit at $r_p = 10 \text{AU}$, and planet to star mass ratio $q \equiv M_p/M_* = 10^{-3}$. Our simulations include the modifications described in Montesinos et al. (2015) that consider

¹ See also Nayakshin et al. (2007) for earlier models on the scale of galactic nuclei.

the planet luminosity and radiative cooling. Additionally, we compute the expected accretion on to the planet, which is used to calculate the planet accretion luminosity. This energy is distributed over the CPD as a heating term in the energy equation. In the following subsections we describe the equations used to quantify each of these ingredients.

2.1 Energy Equation

The energy surface density e is evolved using the equation described in D’Angelo et al. (2003):

$$\frac{\partial e}{\partial t} + \vec{\nabla} \cdot (e \vec{v}) = -P \vec{\nabla} \cdot \vec{v} + Q_{\nu}^+ + Q_p^+ - Q^-, \quad (1)$$

where \vec{v} is the velocity, P is the vertically integrated pressure, Q_{ν}^+ and Q_p^+ are the viscous and planet heating terms, and Q^- is the radiative cooling term. As described in Montesinos et al. (2015), the system is closed with an ideal equation of state for the pressure as a function of mass surface density Σ and mid-plane temperature T :

$$P = \Sigma T \bar{R}, \quad (2)$$

and the energy density is related to the temperature using:

$$e = \Sigma T \frac{\bar{R}}{\gamma - 1}, \quad (3)$$

with the specific gas constant $\bar{R} = k_b / \mu m_H$. The adiabatic index is $\gamma = 1.4$, considering that molecular hydrogen is diatomic, the mean molecular weight is $\mu = 2.35$, and k_b is the Boltzmann constant.

We do not take into account the heating by stellar irradiation, since Montesinos et al. (2015) showed that in the circumplanetary region this effect is always subdominant compared to the planet and viscous heating contributions.

2.2 Viscosity

For the viscosity due to shear in the disc we use the Shakura & Sunyaev (1973) prescription:

$$\nu = \alpha c_s^2 / \Omega_K, \quad (4)$$

where c_s is the sound speed, Ω_K is the keplerian angular velocity, and α is a free parameter that we set to $\alpha = 0.004$.

The energy dissipation due to viscosity contributes to heating the disc through the following term,

$$Q_{\nu}^+ = \frac{1}{2\nu\Sigma} (\tau_{r,r}^2 + \tau_{r,\theta}^2 + \tau_{\theta,\theta}^2) + \frac{2\nu\Sigma}{9} \nabla^2 \vec{v}, \quad (5)$$

which is described in D’Angelo et al. (2003), where $\tau_{r,r}$, $\tau_{r,\theta}$ and $\tau_{\theta,\theta}$ are the elements of the stress tensor.

2.3 Accretion Model

We use the accretion model implemented in FARGO (Masset 2000), which removes gas from the surface density within the Hill radius, using the following radial behavior (Kley 1999; Dürmann & Kley 2017),

$$\frac{d\Sigma_{\text{acc}}}{dt}(r) = \begin{cases} 0 & r = |\vec{r} - \vec{r}_p| > 0.75 R_{\text{Hill}} \\ -\frac{1}{3} \Sigma(r) / t_{\text{acc}} & 0.45 R_{\text{Hill}} < r < 0.75 R_{\text{Hill}} \\ -\Sigma(r) / t_{\text{acc}} & r < 0.45 R_{\text{Hill}}, \end{cases} \quad (6)$$

where the Hill radius is $R_{\text{Hill}} = r_{\text{p}} \sqrt[3]{q/3}$. For convenience we write the accretion timescale in units of the planet orbital time as $1/t_{\text{acc}} = f_{\text{acc}}/T_{\text{p}}$. The accretion fraction f_{acc} can be then understood as which fraction of, or how many times, the circumplanetary region is accreted in one orbit of the planet around the star. The removed disc mass is equal to the accretion rate of the planet,

$$\frac{dM_{\text{p}}}{dt} = \int -\frac{d\Sigma_{\text{acc}}(r)}{dt} dA. \quad (7)$$

In our simulation setup, however, we do not add the accreted mass $\dot{M}_{\text{p}} dt$ to the planet mass, since the final systems would not be dynamically equivalent and therefore, not comparable in the analysis. We only use \dot{M}_{p} to compute the heating that the accretion process produces.

2.4 Planet Heating

The planet heating term Q_{p}^+ is calculated as

$$Q_{\text{p}}^+ = \epsilon f(r) L_{\text{p}}(t), \quad (8)$$

where L_{p} is the total energy released by the planet, $f(r)$ is a smoothing function that distributes the energy within the CPD radius² R_{CPD} , and ϵ is an efficiency factor which can be interpreted as the amount of energy emitted by the planet that is actually absorbed by the gas. For R_{CPD} we follow Crida et al. (2009) and consider $R_{\text{CPD}} = 0.6 R_{\text{Hill}}$. This work uses the same smoothing function described by Montesinos et al. (2015):

$$f(r) = \begin{cases} 0 & r > R_{\text{CPD}} \\ \frac{1}{\pi R_{\text{CPD}}^2} 5 \exp(-5 \frac{r^2}{R_{\text{CPD}}^2}) & r < R_{\text{CPD}}. \end{cases} \quad (9)$$

In our model the planet luminosity is defined as

$$L_{\text{p}}(t) = \frac{1}{2} \frac{GM_{\text{p}}}{R_{\text{p}}} \dot{M}_{\text{p}}(t), \quad (10)$$

considering the change of energy of a test particle in Keplerian motion when accreted at the planet radius R_{p} . For the latter, we take the Jupiter radius.³

2.5 Radiative Cooling

The gas cooling term Q^- accounts for the energy radiated by the gas in the vertical direction considering blackbody emission. We use the same procedure as in Montesinos et al. (2015), computing the optical depth as:

$$\tau = \frac{1}{2} \kappa \Sigma. \quad (11)$$

Our model assumes a constant opacity of $\kappa = 100 \text{ cm}^2/\text{g}$, consistent with the absorption opacities shown by

² With $\int_0^{R_{\text{CPD}}} 2\pi r f(r) dr \approx 1$.

³ Notice that because the gas is accreted from a finite distance ds , the term L_{p} is overestimating the planet luminosity by a factor of $(1 - \frac{R_{\text{p}}}{ds})^{-1}$. The discrepancy is highest for the closest cells, where ds corresponds to the length of the grid cells. For our simulations, the maximum overestimate would be a factor of only 1.007, so we neglect this correction for simplicity. Notice also that the radius of the accreting proto-planet is probably larger than Jupiter's (see e.g., Helled et al. 2014). That can be corrected by choosing a smaller value for the efficiency parameter ϵ .

Kataoka et al. (2015) for grains of sizes $1\mu\text{m}$ to $100\mu\text{m}$. We checked that the CPD region is optically thick throughout all the simulations, to ensure that the planet luminosity does interact with the surrounding material.

To model the emission from the disc surface considering its vertical structure we use Hubeny (1990) prescription for the effective optical depth:

$$\tau_{\text{eff}} = \frac{\sqrt{3}}{4} + \frac{3\tau}{8} + \frac{1}{4\tau}. \quad (12)$$

Then the effective temperature and the cooling term are defined as:

$$T_{\text{eff}}^4 = \frac{T^4}{\tau_{\text{eff}}}, \quad (13)$$

$$Q^- = 2\sigma T_{\text{eff}}^4, \quad (14)$$

where σ is the Stefan–Boltzmann constant and the factor 2 accounts for the upper and lower faces of the disc from which the energy is radiated.

To solve the energy equation including this cooling term we use the implicit solution for the source step, using the same approximations as Commerçon et al. (2011) for the expansion of the power of the temperature.

3 SIMULATION SETUP

3.1 Code Units, Grid Domain and Initial Conditions

We choose as mass unit the mass of the star $M_* = 1M_{\odot}$ and as distance unit the planet orbital radius $r_{\text{p}} = 10 \text{ AU}$. The gravitational constant in code units is $G = 1$, in consequence the planet orbital period is $T_{\text{p}} = 2\pi$ in code units.

The initial surface density profile of the disc is set as:

$$\Sigma(r) = \Sigma_0 \frac{r_{\text{p}}}{r}, \quad (15)$$

with Σ_0 the density at the planet location.

The resolution of our simulations is $n_r \times n_s = 320 \times 960$, with n_r and n_s the number of radial and azimuthal sections respectively. The radial domain goes from 4 AU to 25 AU from the star. At the inner radius we set an open boundary condition, while at the outer radius we impose a constant surface density.

3.2 Smoothing Tapers

To smoothly introduce the effect of the planet gravity the code uses a taper factor, such that the planet mass increases from $q = 0.0$ to $q = 10^{-3}$ within $N_{\text{taper}} = 10$ orbits.

$$M_{\text{p}}(t) = \begin{cases} M_{\text{p}} \cdot \sin^2\left(\frac{\pi}{2} \frac{t}{N_{\text{taper}} T_{\text{p}}}\right) & t < 10 T_{\text{p}} \\ M_{\text{p}} & \text{otherwise,} \end{cases} \quad (16)$$

The system is evolved for 100 orbits before letting the planet accrete, in order to avoid high accretion rates previous to the gap opening. The accretion fraction f_{acc} and the planet luminosity L_{p} are also multiplied by a taper of the same form between the orbits 100 and 110, to introduce their effect smoothly.

Table 1. Parameter space

Σ_0 (g/cm ²)	15, 30, 45
f_{acc} ($= T_p/t_{\text{acc}}$)	0.33, 0.5, 1.0, 2.0
ϵ	0.0, 0.04, 0.1, 0.4, 1.0

3.3 Parameter Space

Our simulations explore the parameter space for: the initial surface density Σ_0 , the accretion fraction f_{acc} , and the planet heating efficiency ϵ . The different values for ϵ are used to take into account that it is not known how much of the energy released by the planet will be absorbed by the gas. This value is expected to decrease for CPDs that are either optically or geometrically thinner.

For the accretion timescale of the planet, the values used are between the viscous and the free-fall time-scales of the CPD, and moreover correspond to the accretion rates around our range of interest, above of $10^{-9}M_{\odot}/\text{yr}$.

For Σ_0 , the different simulations use values of 15, 30 and 45 g/cm². For reference, a disc with $\Sigma_0 = 30$ g/cm² extending from 1 AU to 50 AU has a mass of approximately $10^{-2}M_{\odot}$. We find that this interval of densities produces accretion rates in our range of interest ($\dot{M}_p \sim 10^{-9} - 10^{-8} \frac{M_{\odot}}{\text{yr}}$). Less massive disc have lower accretion rates and become optically thin, escaping the scope of our model. Table 1 lists all parameters used.

4 ON THE CPD AND THE PLANET

In this section we present the results of our simulations in the local region around the planet, namely the planet accretion rate and luminosity, and also the CPD properties. We present the fiducial simulations, and study the results variation with the free parameters (Σ_0 , f_{acc} , ϵ). Additional simulation setups will only be used to confirm some of the properties spotted in the fiducial simulations. In order to avoid possible biases due to time variability, the presented results are taken from the last 100 snapshots averaged between the orbits 300 and 350 (unless a particular time is explicitly mentioned). Notice the snapshots are separated by an interval of 1/2 of the planet orbit.

To start the results section we present a comparison of the density and temperature distributions between the case with $\epsilon = 1.0$ and the case with $\epsilon = 0.0$ (Figures 1 and 2), using the residuals $(\Sigma(\epsilon_1) - \Sigma(\epsilon_0))/\Sigma(\epsilon_0)$, and $(T(\epsilon_1) - T(\epsilon_0))/T(\epsilon_0)$. Through the following sections most results will be associated with these two maps, so it is useful to introduce them at this point. In the CPD, the plots show that the feedback reduces its mass and increases its temperature, while in the gap both the density and the temperature are increased.

4.1 Planet Accretion

Arguably, the most important quantities in our study are the planet accretion rate and luminosity, which can be indirectly measured by observations, potentially revealing the presence of a planet. A direct detection of the planet brightness is unlikely at this stage, since we expect it to be embedded

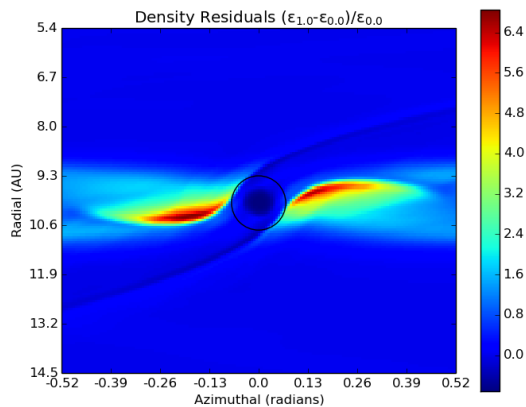


Figure 1. Surface density comparison between the case $\epsilon = 1.0$ and $\epsilon = 0.0$, using the residual $(\Sigma(\epsilon_1) - \Sigma(\epsilon_0))/\Sigma(\epsilon_0)$. Both simulations have $\Sigma_0 = 30\text{g/cm}^2$ and $f_{\text{acc}} = 1.0$. The plot shows that the simulation with $\epsilon = 1.0$ has less mass in the CPD, and more mass in the gap region than the case with $\epsilon = 0.0$. The Hill radius around the planet is marked with a black circle.

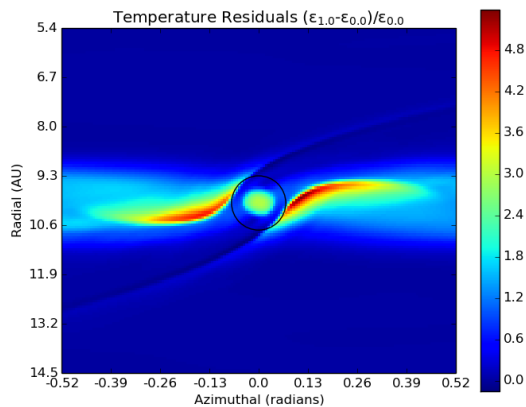


Figure 2. Same as Fig. 1, but showing the temperature residual, $(T(\epsilon_1) - T(\epsilon_0))/T(\epsilon_0)$. The plot shows that the simulation with $\epsilon = 1.0$ reaches higher temperatures both in the CPD region and inside the gap.

in an optically thick CPD. Moreover, the planet surface is too small to be resolvable, and would be confused with the surrounding gas.

Our results show that the accretion onto the planet is determined primarily by the surface density Σ_0 – more massive discs provide a bigger reservoir of material to feed the circumplanetary disc and the planet itself (Figure 3). The values of the accretion rate go from $10^{-9}M_{\odot}/\text{yr}$ to $5 \cdot 10^{-8}M_{\odot}/\text{yr}$, and produce planet luminosities above $10^{-4}L_{\odot}$ and up to almost $10^{-2}L_{\odot}$. As expected from Eqs. (6) and (7), for larger accretion fractions f_{acc} (shorter accretion timescales t_{acc}) \dot{M}_p increases by a factor of a few. However, the main feature of the plot is the drop in the accretion rate when the planet feedback is turned on. For the different disc masses the feedback causes an average decrement in the ac-

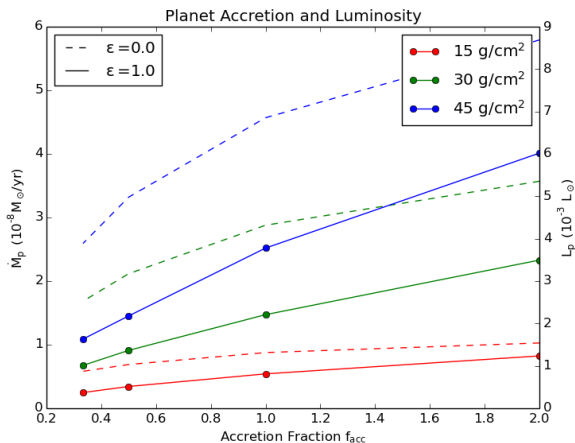


Figure 3. Planet accretion rate (left axis) and luminosity (right axis) as function of the accretion fraction f_{acc} , for different values of Σ_0 . Solid lines are for $\epsilon = 1.0$ and dashed lines for $\epsilon = 0.0$. In all our cases the planet accretion rate has values above $10^{-9} M_{\odot}/\text{yr}$.

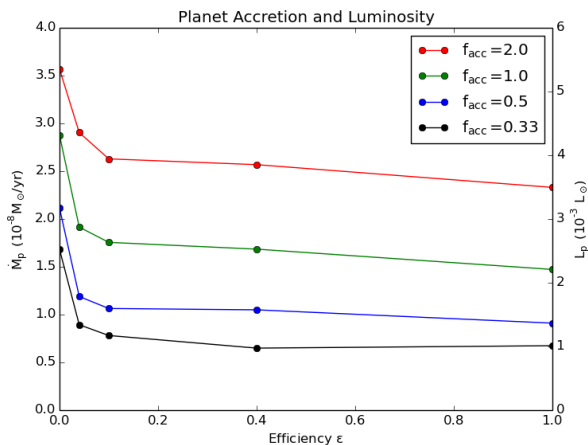


Figure 4. Planet accretion rate (left axis) and luminosity (right axis) as a function of the feedback efficiency ϵ , for different values of f_{acc} , with $\Sigma_0 = 30 \text{ g/cm}^2$. The plot shows the monotonic decrease of M_{p} with ϵ . Most of the variation occurs at low efficiencies, and stays roughly constant for $\epsilon \gtrsim 0.1$.

cretion rate between 37%- 47%, relative to the accretion rate of the planet when no feedback is considered. Figure 4 shows that most of this effect takes place at efficiencies as low as $\epsilon \leq 0.1$, and remains approximately constant from there to $\epsilon = 1.0$. This is interesting because even if the feedback is not 100% efficient, or if the calculation of the planet luminosity is overestimated by any reasons, the feedback would still be effective, dropping the accretion rate and luminosity to a floor value. The drop in accretion can be linked to the density conditions in the CPD, because of Eq.(6), which will be addressed in the following section.

So far our results show that the detectable luminosities, studied by Zhu (2015), are possible, and the feedback is not able to completely stall the planet accretion rate.

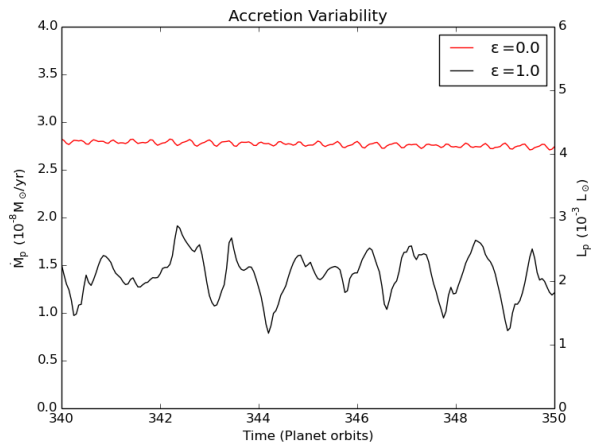


Figure 5. Planet accretion rate (left axis) and luminosity (right axis) as a function of time, with $f_{\text{acc}} = 1.0$ and $\Sigma_0 = 30 \text{ g/cm}^2$. The plot shows the variation in the accretion during the last 10 orbits of the simulation for the cases with the feedback turned on and off.

4.1.1 Time Variability

Another interesting quantity from the observational point of view is the variation of the planet accretion and luminosity with time. If the variations are too intense, then observed planet signatures might not be good indicators of the planet properties. Figure 5 shows the variability of the planet accretion during the last 10 orbits of the simulation. The standard deviation is around 1% when the feedback is turned off, and around 15% when turned on. If measurements of accretion luminosity variability are obtained, it would be important to consider that this can be caused by the planet feedback, and not only by the eccentricity of its orbit (Dunhill 2015).

4.2 Circumplanetary disc

The CPD is responsible of providing material to the accreting planet, and is the region that will be immediately affected by the planetary feedback. We will now study how its properties behave under the effect of the planet accretion and its feedback.

The mass of the CPD, shown in Fig. 6, goes between $10^{-4} - 10^{-3} M_{\text{p}}$, mainly determined by the protoplanetary disc density, and decreasing for higher accretion fractions, as more mass is removed at each timestep. Figure 7 (see also Fig. 1) shows how the feedback acts depleting the CPD region with increasing efficiencies, which drives the reduction on the planetary accretion rate. The depletion can be understood as a result of the higher pressure in the CPD region when the feedback is implemented. This produces a steeper pressure gradient, thus a greater force that pushes the material outside the CPD. The pressure gradient continues to keep the material from reentering the CPD. This process was already discussed by Montesinos et al. (2015), showing that the feedback alone can stop the material from accumulating near the planet, even when accretion is not considered.

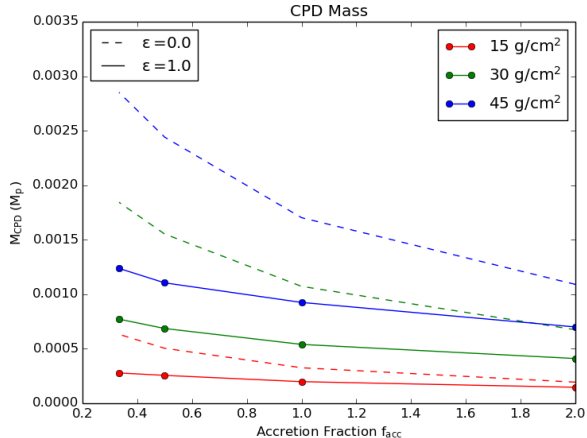


Figure 6. Circumplanetary disc mass as a function of the accretion fraction f_{acc} , for different values of Σ_0 . Solid lines are for $\epsilon = 1.0$ and dashed lines for $\epsilon = 0.0$. The CPD masses have values in the range $M_{\text{CPD}} \sim 10^{-4} - 10^{-3} M_{\text{P}}$. M_{CPD} decreases for higher f_{acc} since more gas is removed from the disc.

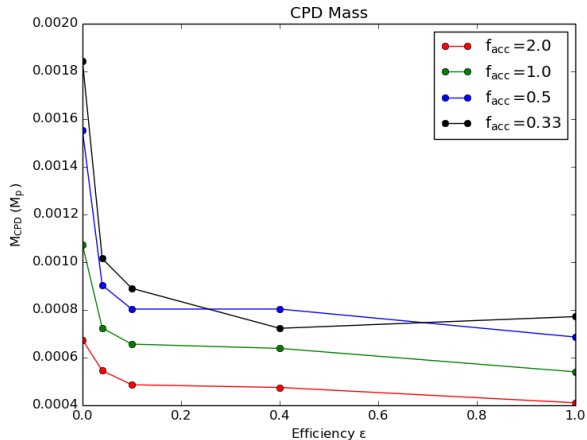


Figure 7. Circumplanetary disc mass as a function of the feedback efficiency ϵ , for different values of f_{acc} , with $\Sigma_0 = 30 \text{ g/cm}^2$. For increasing efficiencies we typically obtain a less massive CPD, with the material escaping from the planet potential.

4.2.1 Temperature and Luminosity

The planetary feedback causes a raise in the CPD temperature which can be seen in the temperature residual map (Figure 2), and in more detail in Figure 8. The CPD temperature raises with the heating term Q_{p}^+ , which is increased by both planet accretion \dot{M}_{p} and feedback efficiency ϵ . The temperature when the feedback is turned off lies between 150–200 K, and raises to 400–1100 K depending on the planet luminosity. These values are consistent with those obtained by Montesinos et al. (2015), and also by Szulágyi et al. (2017) for the core accretion model.

Along with the temperature, the feedback also increases the CPD scale height. Even though our models are two-dimensional, we can estimate the aspect ratio of the CPD as $(h/d)_{\text{CPD}} = c_{\text{s}}/v_{\text{k}}$, with the adiabatic sound speed $c_{\text{s}} = \sqrt{\gamma(\gamma - 1)\epsilon/\Sigma}$, and the Keplerian velocity of the CPD

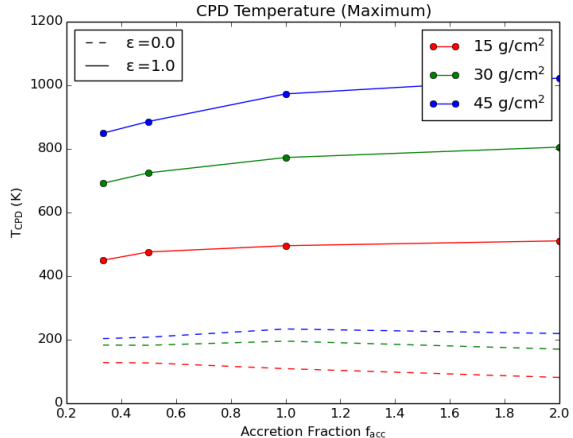


Figure 8. Maximum temperature in the CPD region as a function of the accretion fraction, for different values of Σ_0 . Solid lines show the models with $\epsilon = 1.0$ and dashed lines those with $\epsilon = 0.0$. More massive discs and higher accretion fractions are direct cause for higher planet luminosities, which produce the raise in the CPD temperature up to $\sim 1000 \text{ K}$.

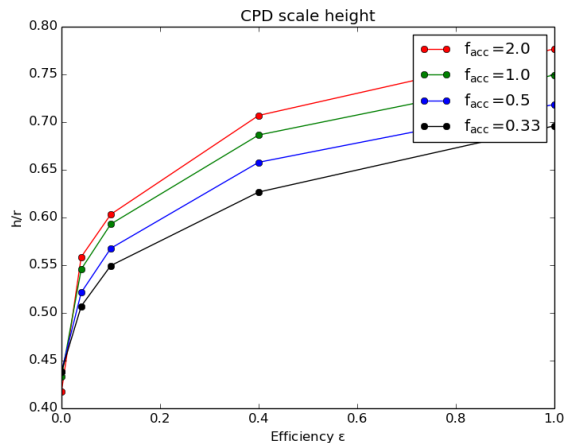


Figure 9. Average scale height of the CPD as a function of the feedback efficiency ϵ , for different values of f_{acc} , with $\Sigma_0 = 30 \text{ g/cm}^2$. For higher efficiencies more energy is absorbed by the gas, producing higher temperature and scale height for the CPD.

around the planet potential $v_{\text{k}} = \sqrt{GM_{\text{p}}/d}$, with d the distance to the planet. Figure 9 shows the average scale height $(h/d)_{\text{CPD}}$ inside the CPD region for different simulations. As the temperature grows for higher ϵ , the sound speed of the gas also increases making the CPD thicker, reaching values in the range 0.4–0.7 for the cases with $\epsilon = 1.0$.

Finally, we show the bolometric luminosity of the CPD and its spectrum in Figures 10 and 11. These estimates assume that the CPD emits as a multi-colour blackbody, with the vertical structure modeled through Eqs. (12) and (13) to obtain the effective temperature. As our simulations are limited by the grid resolution, we can only integrate the CPD luminosity down to $\sim 100R_{\text{J}}$ from the planet. This causes the inner region of the disc, which is the hottest and brightest, to be omitted from our calculation of the planet

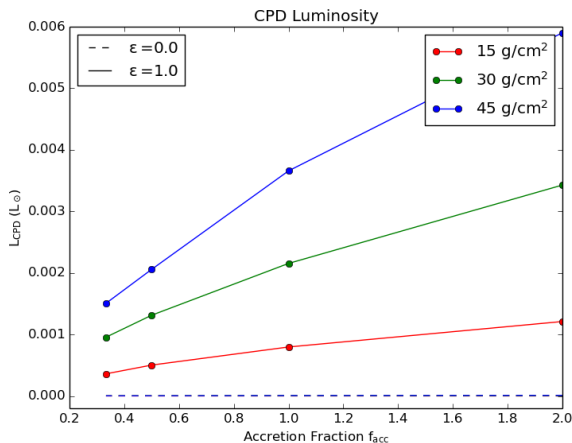


Figure 10. CPD bolometric luminosity as a function of the accretion fraction, for different values of Σ_0 . Solid lines show models with $\epsilon = 1.0$, while dashed lines show $\epsilon = 0.0$. Similarly to the previous plots, higher Σ_0 and f_{acc} produce an increase in the luminosity of the planet, which translates in a raise of the CPD luminosity that can reach values up to $5 \times 10^{-3} L_{\odot}$. This plot considers only a single face of the CPD, as would be seen by a face-on observer. Moreover, the luminosity only considers the part of the disc directly resolved by our simulations, down to $\approx 100 R_J$ (cf. Fig. 11).

luminosity and spectra. Nevertheless, we describe sub-grid calculations of the inner CPD spectrum below.

Studying the regions that we can resolve, for the case with $\epsilon = 1.0$ the CPD luminosity (of a single face) can be as bright as the planet. This means that the CPD is radiating around twice the planet luminosity. Recall that the planet luminosity is not the only energy source for the CPD. The latter is also heated through by viscous dissipation Q_{ν}^+ and pressure work. Therefore it would not be surprising that L_{CPD} raises non-linearly with L_{p} .

Figure 11 shows the spectral flux distribution expected from a face-on CPD located at a distance of 100 pc, in the model with $\Sigma_0 = 30 \text{ g/cm}^2$ and $f_{\text{acc}} = 1.0$. The maximum flux, considering only the resolved, or “feedback” component, is 11 mJy at around $23 \mu\text{m}$, which is achieved for $\epsilon = 1.0$. In addition to the spectra obtained from the simulations, we also include in the plot a sub-grid “accretion” component. This is defined as the multi-colour black body flux of a $2R_J$ to $250R_J$ accretion disc, with a temperature profile calculated from the corresponding accretion rate onto the planet (see Eisner 2015; Frank et al. 2002, eqs. 5.43, 5.45)⁴. We can see in the case with the highest feedback efficiency ($\epsilon = 1.0$) that its MIR signature can be brighter than that due to accretion alone. Adding up both the feedback and accretion components in the MIR, the total signal would be above 15 mJy at $\lambda \approx 20 \mu\text{m}$. Even at lower, perhaps more realistic efficiencies ($\epsilon = 0.1$), the combined signal remains above 5 mJy in the MIR, and the spectrum shows a broader shape due to the combination of both effects. The relatively high flux obtained from our models makes CPDs interesting

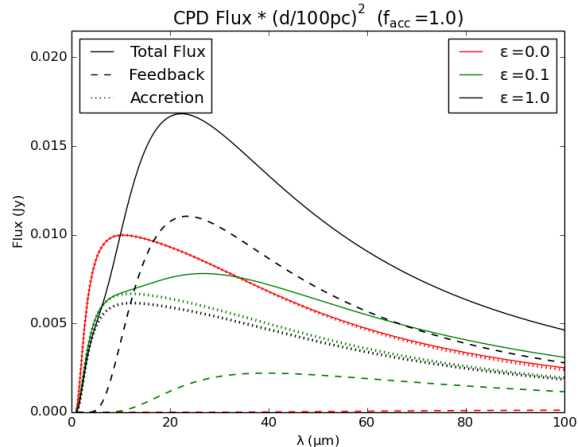


Figure 11. Spectra for a CPD located at 100 pc, assuming blackbody emission, for a disc with $\Sigma_0 = 30 \text{ g/cm}^2$ and $f_{\text{acc}} = 1.0$, for three different feedback efficiencies. The dashed lines show the spectra obtained directly from our feedback simulations, while the dotted lines show the sub-grid emission of the inner $250 R_J$ of the CPD calculated using the corresponding accretion rate for each efficiency. The solid lines show the sum of these two models. The maximum flux is reached when the feedback is completely turned on ($\epsilon = 1.0$), with $F \sim 17 \text{ mJy}$ at $23 \mu\text{m}$. As in the previous plot, this is the emission of a single face of the CPD.

targets for future MIR observations, for example using the Mid-Infrared Instrument (MIRI) on JWST, which at $20 \mu\text{m}$ requires a signal of 1 mJy to obtain a signal-to-noise of 10 for an observation time of 10^4 seconds (Rieke et al. 2015; Glasse et al. 2015).

As for the planet itself, for the same model and assuming a blackbody of Jupiter radius, it would have a temperature of $T_{\text{p}} = 3850 \text{ K}$ with a peak flux of 0.6 mJy at $1.2 \mu\text{m}$.

5 ON THE GAP STRUCTURE

Although the gap is not directly involved in our numerical implementation of accretion feedback, it can be affected by this process through the transport of mass and energy from the CPD region. In this section we will show the different effects of the planetary accretion and feedback in the gap properties.

5.1 Density and Temperature

The effect of accretion on the density profile was shown by Dürmann & Kley (2015), using an equivalent prescription for the accretion rate. In their results the accretion deepened the gap carved by a planet, when compared with the non-accreting case. Our results in Figure 12 show the same behavior in the density profiles, for higher accretion fractions f_{acc} more mass is removed, deepening the gap. When the accretion is turned off, the mass that would otherwise be accreted by the planet accumulates on the CPD. If the CPD is “full”, we expect the gas to go back to the coorbital region. In order to easily compare different models, we do not add the accreted material to the planet mass. If that was

⁴ Following Zhu (2015), we ignore the direct effect of the planet luminosity on the inner CPD disc dynamics. Feedback influences this region only by setting the accretion rate throughout the disc.

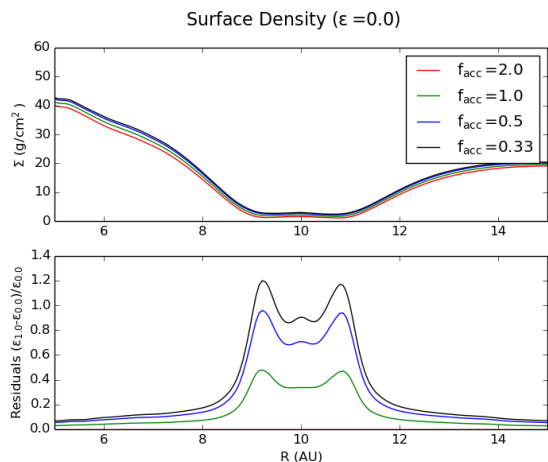


Figure 12. Top: Azimuthally averaged density profiles for discs with $\Sigma_0 = 30 \text{ g/cm}^2$ and $\epsilon = 0.0$. Bottom: Residuals normalized respect to the $f_{\text{acc}} = 0.0$ curve of the top panel. We can see how the overall density in the gap is reduced for higher accretion fractions, since more mass is removed from the simulation.

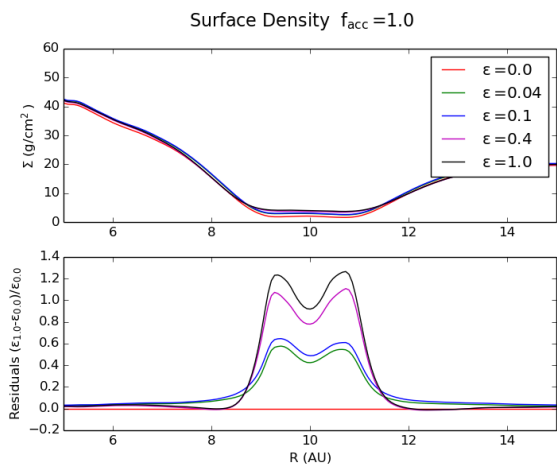


Figure 13. Top: Azimuthally averaged density profiles for discs with $\Sigma_0 = 30 \text{ g/cm}^2$ and $f_{\text{acc}} = 1.0$. Bottom: Residuals normalized respect to the $\epsilon = 0.0$ curve of the top panel. We can see an increase in the density of the gap region for higher efficiencies ϵ .

the case, higher f_{acc} would produce more massive planets, which in turn would carve even deeper gaps.

More interesting is the effect of the feedback on the density profile. In the density residual map (Figure 1) it can be seen that not only the CPD is depleted when the planet luminosity is considered, but also that the gap becomes more dense – we will refer to this as “partially refilled”. This increase in the density not only happens in the regions that are immediately outside the Hill radius, but in the whole azimuthal range. In Figure 13 we can see that for higher efficiencies ϵ the whole gap density is increased. The physical reason for this effect is not intuitive at all, but it was also seen in Szulágyi (2017)’s 3D simulations when switching the planet temperature. We will try to decompose it into the sum of partial effects that can be explained with our prior knowledge.

Before beginning it is necessary to recall two points: the effect of the accretion onto the gap density (Fig. 12), and the effect of feedback in the raise of temperature of the whole coorbital region. The latter can be seen in the residual temperature map (Figure 2), and also in the temperature profiles (Figure 14), that show an increment from approximately 12 K to 35 K when the feedback is turned on, an effect that was also found by Montesinos et al. (2015). Our first candidate for the refilling of the gap is the coupling between the feedback and the accretion rate. Recalling Figure 4, when the feedback is turned on the accretion rate is reduced. Then, if the accretion rate is reduced, the gap is refilled. To test this effect we use a new set of simulations in which we set a fixed accretion rate of $\dot{M}_p = 10^{-8} M_\odot/\text{yr}$. If the variable accretion was responsible for the refilling, then by setting it constant the effect should disappear. Our results for these simulations are shown in Figure 15, which shows that the partial refilling is still present, although with less intensity (around a factor of 1/3) than in the case with our fiducial prescription for the accretion rate. The next candidate is the viscous torque, which directly counteracts the planet torque, and is proportional to the viscosity. From the α prescription (Eq. 4) we can see that the viscosity increases with the sound speed c_s . Therefore the increment in the temperature translates in an increment in the viscous torque which may contribute to refill the gap. To test this we use another set of simulations with a constant viscosity of $\nu = 2 \cdot 10^{-5}$ (in code units), equivalent to the one obtained with the α prescription in the sense that the shape and depth of the gap are as similar as possible with the case with no feedback and constant accretion rate, while trying to keep also the global density profiles similar.⁵ Then, our set of simulations with constant ν and \dot{M}_p should reveal if the viscous torque is closing the gap. Figure 16 shows however, that the refilling of the gap is still present, almost with the same intensity that in the case with the α viscosity and constant accretion. Although the trend is not so clear as in the previous cases, the simulation with $\epsilon = 1.0$ is the best indicator that the gap is still refilled even for constant viscosity, and that there must be other effects involved. To quantify the influence of accretion and viscosity in the gap refilling, in Figure 17 we compare the test simulations with constant accretion to the fiducial simulations (the simulations with $f_{\text{acc}} = 0.5$ and $f_{\text{acc}} = 1.0$ were used since these have the most similar accretion rates and disc conditions to the test simulations). The figure shows how a constant accretion produces less variation in the gap density under similar conditions in the planet luminosity, and allows to determine that the accretion is responsible for approximately 60% of the variation, while the viscosity can be responsible only for a 10% of the variation. While there is a fraction of the gap refilling that remains unexplained, we can attribute it to a non-linear combined effect, or to the turbulence generated when the feedback is turned on.

⁵ The value for the viscosity was obtained through trial and error, and reproduces the depth of the gap with a difference of less than 1 g/cm^2 (or 30%).

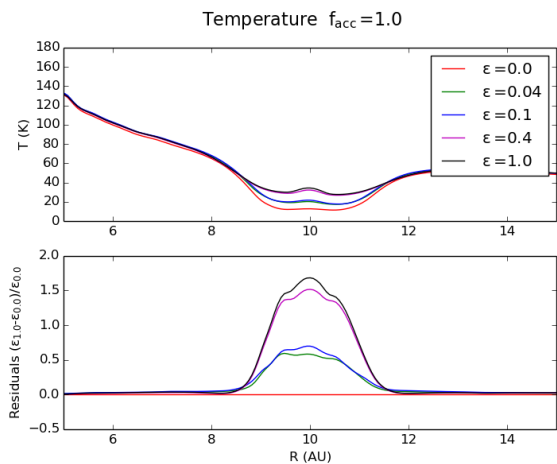


Figure 14. Top: Azimuthally averaged temperature profiles for discs with $\Sigma_0 = 30 \text{ g/cm}^2$ and $f_{\text{acc}} = 1.0$. Bottom: Residuals normalized respect to the $\epsilon = 0.0$ curve of the top panel. We can see an increase in the temperature of the gap region for higher efficiencies ϵ , with a peak at the planet orbit.

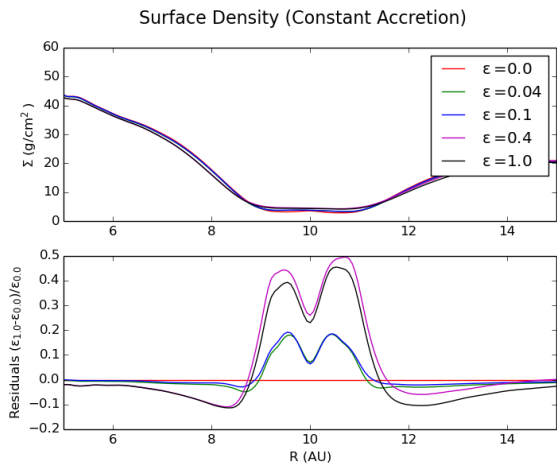


Figure 15. Top: Azimuthally averaged density profiles for discs with $\Sigma_0 = 30 \text{ g/cm}^2$ and a constant accretion rate of $10^{-8} M_{\odot}/\text{yr}$. Bottom: Residuals normalized respect to the $\epsilon = 0.0$ curve of the top panel. We can see an increase in the density of the gap region for higher efficiencies ϵ , although with less intensity than in our fiducial simulations.

5.2 Pressure and Velocity

Now we will discuss the effect of the feedback on the pressure and azimuthal velocity of the gas in the coorbital region. Besides the increase in the temperature of the coorbital region, there is also an increment in the thermal energy, which is proportional to the gas pressure. Figure 18 shows how the thermal energy increases with ϵ . An increment in the pressure at the gap region causes a shallower pressure gradient, and reduces the contribution of the pressure component in the gas acceleration. Figure 19 shows how the magnitude of the acceleration caused by the pressure is reduced for higher values of ϵ , while maintaining its direction (positive at the inner border, and negative at the outer border of the gap). The effect can be directly seen in the azimuthal velocity pro-

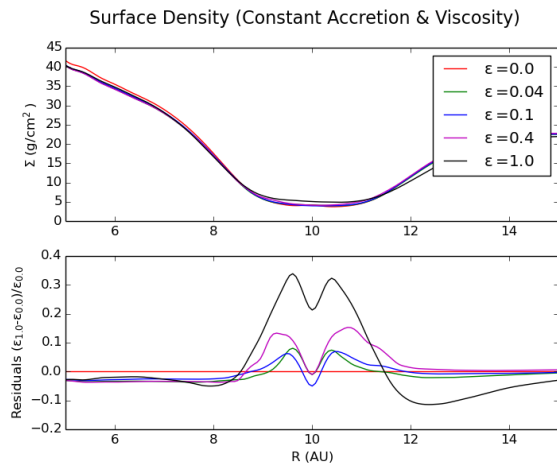


Figure 16. Top: Azimuthally averaged density profiles for discs with $\Sigma_0 = 30 \text{ g/cm}^2$, a constant accretion rate of $10^{-8} M_{\odot}/\text{yr}$ and constant viscosity. The viscosity ν was selected to replicate the simulations with α viscosity. Bottom: Residuals normalized respect to the $\epsilon = 0.0$ curve of the top panel. We can see an increase in the density of the gap region for higher efficiencies ϵ , although the trend is less noticeable in this case.

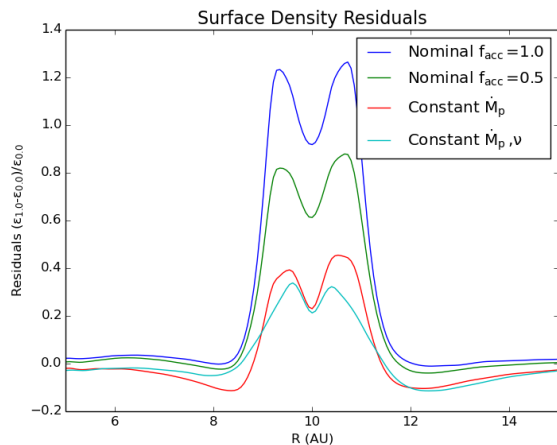


Figure 17. Azimuthally averaged residuals of density profiles with different setups. The curves are the residuals of simulations with $\epsilon = 1.0$ relative to $\epsilon = 0.0$ using the same setup. All the simulations are discs with $\Sigma_0 = 30 \text{ g/cm}^2$, but with different accretion prescriptions. The two fiducial simulations use the accretion fraction prescription with $f_{\text{acc}} = 1.0$ and $f_{\text{acc}} = 0.5$, the two simulations with a constant accretion rate of $10^{-8} M_{\odot}/\text{yr}$ use the fiducial α viscosity, and a constant viscosity of $\nu = 2 \times 10^{-5}$ (in code units).

file in Figure 20, where the azimuthal velocity takes values closer to the Keplerian velocity when the feedback is on. Notice that at the inner border of the gap the gas orbits at sub-Keplerian speed, and in the outer border at super-Keplerian, due to the pressure gradient at the gap borders. Although the azimuthal velocity differs from Keplerian only by a 2% for $\epsilon = 0.0$, and 1% for $\epsilon = 1.0$, this contribution is very significant compared to the variation caused by the gas pressure alone in a disc with no planet, where the variation is just 0.1–0.2%, as can be seen far away from the planet po-

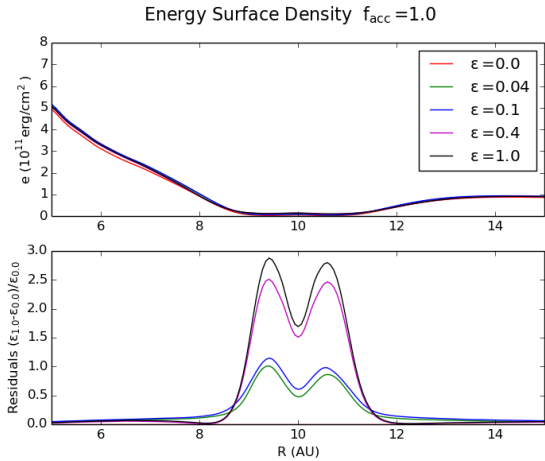


Figure 18. Top: Azimuthally averaged energy profiles with $\Sigma_0 = 30 \text{ g/cm}^2$ and $f_{\text{acc}} = 1.0$. Bottom: Residuals normalized respect to the $\epsilon = 0.0$ curve of the top panel. For higher feedback efficiencies, the planetary heating produces an increment in the energy surface density in the gap region.

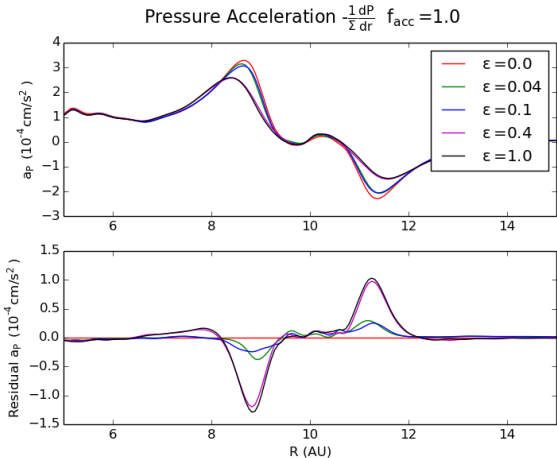


Figure 19. Top: Azimuthally averaged radial pressure acceleration with $\Sigma_0 = 30 \text{ g/cm}^2$ and $f_{\text{acc}} = 1.0$. Bottom: Residuals respect to the $\epsilon = 0.0$ curve of the top panel. The plot shows how the higher feedback efficiencies tend to smooth out the pressure gradient. At the inner and outer edges of the gap the pressure acceleration becomes less positive and less negative, respectively.

tential. A change in the orbital velocity has a direct impact on the dust drift, which is affected even by small variations in the gas velocity (see § 6.2).

5.3 Vortensity

The last effect of the feedback to be explored in this work is on the vortensity. This quantity measures the local rotation of the fluid at every point, and is defined as:

$$\vec{\omega} = \frac{\nabla \times \vec{v}}{\rho}, \quad (17)$$

with the gas volume density estimated as $\rho = \Sigma/h$. Since our simulations are 2D, we only refer to the vertical component of $\vec{\omega}$. In Figures 21 and 22 we see vortex like structures

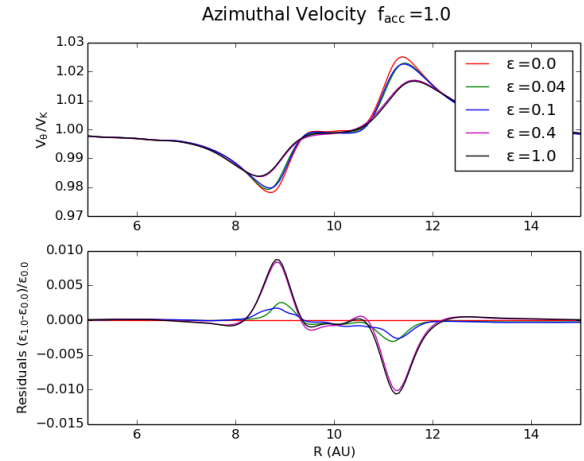


Figure 20. Top: Azimuthally averaged orbital velocity of the gas with $\Sigma_0 = 30 \text{ g/cm}^2$ and $f_{\text{acc}} = 1.0$, normalized to the local Keplerian velocity. Bottom: Residuals normalized respect to the $\epsilon = 0.0$ curve of the top panel. From the residuals we can see the effect of the pressure gradient on the orbital velocity, increasing it at the inner edge, and reducing it at the lower edge. The variation due to the presence of the planet feedback is around 1% of the Keplerian value.

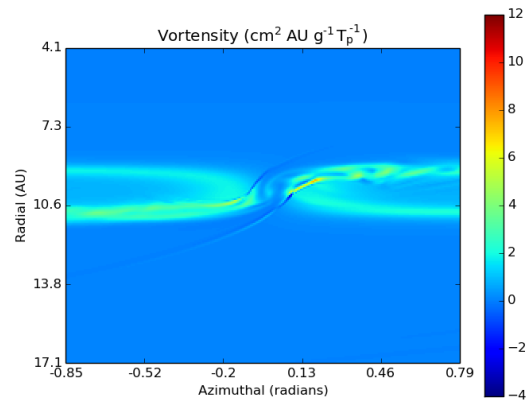


Figure 21. Vortensity map for a simulation with $\epsilon = 0.0$, $\Sigma_0 = 30 \text{ g/cm}^2$ and $f_{\text{acc}} = 1.0$, at a time of 350 orbits. Only small structures appear at the borders of the gap.

appear when the feedback is turned on. These vortices form near the planet, approximately at the Hill radius, before being transported along the borders of the gap. They are short lived, and dissipate before completing a single orbit. The vortensity for the case with $\epsilon = 0.0$ shows less structure and a smoother profile.

We believe the vortices originate due to perturbations in the pressure and density near the planet, produced by the accretion feedback. A thorough analysis of this effect goes beyond the scope of this paper.

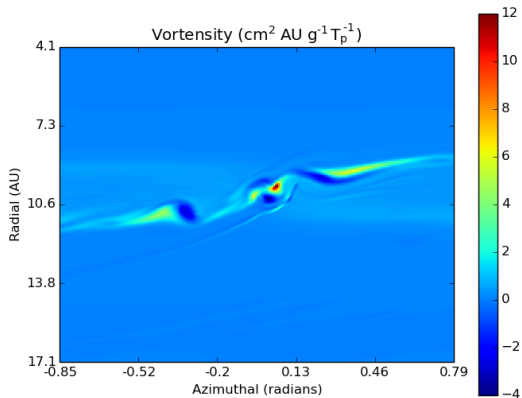


Figure 22. Vortensity map for a simulation with $\epsilon = 1.0$, $\Sigma_0 = 30 \text{ g/cm}^2$ and $f_{\text{acc}} = 1.0$, at a time of 350 orbits. We can notice vortex like structures in the inner and outer edges of the gap. After analyzing multiple snapshots we see that these structures last around an orbit before dissipating and do not appear in simulations without planetary feedback.

6 DISCUSSION

Our simulations showed the diverse effects of feedback from an accreting planet on the CPD and the coorbital region. The most relevant results are that Jupiter-like planets can still achieve detectable accretion rates, and that their heating affects the whole gap, not only the CPD region. Therefore, the infrared emission associated to this process could be used as a tracer for accreting planets.

In the rest of this section we discuss some consequences of our results, and also the limitations of our model.

6.1 Feedback as a Slow Down Mechanism for Accretion

In the core accretion model (Pollack et al. 1996), Jupiter mass planets can enter into a runaway accretion phase, being able to double their masses on timescales as short as 10^4 yr . In the disc fragmentation scenario (Boss 1997), planets typically also grow very quickly, reaching the brown dwarf regime (Stamatellos 2015, but see also Nayakshin (2015)).

It is interesting to note that in our model feedback acts as a limiting mechanism for planet growth, cutting the accretion rates between 37%–47% (see Figures 3, 4), and depleting the CPDs in a similar amount.

6.1.1 Are high feedback efficiencies valid?

This question is crucial for the validity of our model, since our results depend on the planet accretion energy being actually absorbed by the CPD. However, an efficiency factor as low as $\sim 10\%$ is enough for the feedback to have a strong effect (see Figs. 4, 7).

Obtaining a realistic value for the efficiency would require a more sophisticated numerical approach, including a treatment of radiative transfer. Still, we can provide two simple arguments to justify that the radiation of the planet should be absorbed at least partially by the gas. The first one

is the geometry of the CPD, Szulágyi et al. (2016) has shown that the scale height of the disc increases for high feedback values, even to the point of turning the disc into an envelope. Our own 2D models show that the temperature reaches its maximum at the location of the planet. Therefore, we can expect that most of the radiation will go through the gas. Additionally, whether the radiation is absorbed depends on the optical thickness of the gas. A high enough optical depth was already seen by Ayliffe & Bate (2009a,b), and confirmed in the simulations of Szulágyi et al. (2016), which use the flux-limited diffusion approach. From these previous studies we are confident that the feedback efficiency ϵ should have values large enough in order for feedback to be relevant.

6.2 Possible Effects On Dust Drift

Besides the effect of the feedback on the gas, which we have modelled here, we can also expect the dust to be affected by the changes in the gas dynamics. While dust grains follow Keplerian orbits, gas also feels pressure forces, which makes its orbit slightly non Keplerian. If the gas is sub-Keplerian, then the dust grains will lose angular momentum when going through the gas, and drift inwards as a result. In the opposite case, if the gas is super-Keplerian, dust will drift outwards. In terms of the pressure, this can be seen as the dust concentrating at the pressure maxima (Weidenschilling 1977; Pinilla et al. 2012), commonly referred to as “climbing the pressure gradients”.

The analysis of the gas orbital speed and pressure gradients (Figures 19 and 20) let us infer how the dust grains behave. Our simulations show that when the feedback is turned on, the pressure gradient is smoother and the orbital velocity becomes more Keplerian. At the inner edge of the gap, where the pressure gradient is negative, dust drift should be inwards, but slower than in the case with a planet without feedback. The outer edge is more interesting, since here the gas is super-Keplerian, which would allow for dust particles to drift outwards and concentrate at the local pressure maximum outside the carved gap (Rice et al. 2006). Our results however, show that this concentration should be less efficient, and therefore reduce the expected contrast in observations (Fouchet et al. 2007).

Figure 23 shows the expected dust drift due to the pressure gradient component $v_{r,\text{dust}} = (St^{-1} + St)^{-1} \partial_r P / (\Sigma \Omega)$, for the particles with $St = 1$. The drift component caused by the gas radial velocity (which is one order of magnitude lower than the pressure gradient component) was omitted in this calculation, because $v_{r,\text{gas}}$ depends on the underlying surface density distribution. In particular, our initial conditions for the density profile correspond to positive radial velocities in the gas, which are not typical for this type of study and complicate the interpretation of our results. While for $St \geq 1$ particles the gas radial velocity contribution is not as important, for smaller particles it becomes the dominant term, and would require a more appropriate treatment. We also neglected the effect of *radiative* pressure due to the planet luminosity, which is expected to keep small grains outward of the planet (Owen 2014).

In summary, when the feedback is turned on particles will drift slower, both toward the star and to the pressure maximum in the outer edge of the gap, and the particles most affected by the drift will have bigger sizes. The vor-

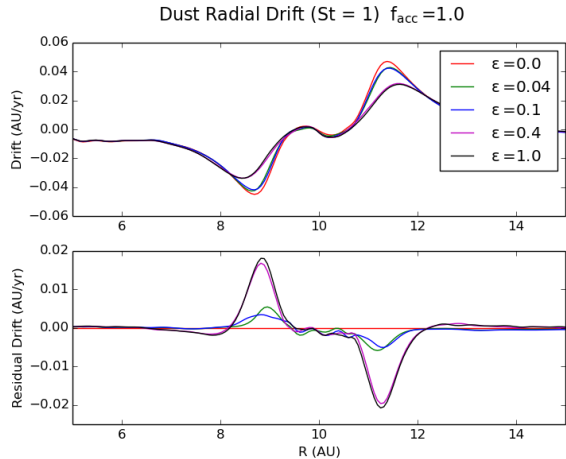


Figure 23. Top: Azimuthally averaged drift velocity of the dust with $\Sigma_0 = 30\text{g/cm}^2$ and $f_{\text{acc}} = 1.0$. The plot shows how the feedback decreases the magnitude of the dust drift as a consequence of smoothing the pressure gradient. The particles with $St = 1$ (corresponding to sizes between 1 – 2 cm) are the most affected by the drifting, which will be less efficient by the effect of the planet luminosity. Bottom: Residuals respect to the $\epsilon = 0.0$ curve of the top panel.

tex structures found when the feedback is turned on could also act as dust traps (Raettig et al. 2015), but the short lifetimes and dissipation make difficult to quantify their impact on dust growth. A detailed analysis of the impact of the feedback in the dust drifting appears to be a promising topic for future studies.

6.3 Model limitations

The weakest point of our model is the lack of the third spatial coordinate. The recent 3D studies of Szulágyi et al. (2014, 2016) have shown the accretion from the CPD onto the planet has a large meridional component caused by the enhancement of the CPD scale height. With our 2D model (and assuming vertical hydrostatic equilibrium) we also see that the scale height increases with the planet luminosity. Further 3D effects, such as the formation of a circumplanetary envelope (Szulágyi et al. 2016; Szulágyi 2017), cannot be followed with our approach.

Previous works have studied the effect of radiative feedback on the migration of the forming planet (Nayakshin & Cha 2013; Stamatellos 2015; Benítez-Llambay et al. 2015). In our models the planet radius was kept fixed, so migration cannot be directly measured from the simulations. A post-processing measurement of the torque acting on the planet was unfortunately inconclusive. The torque magnitude, and even its sign, depended very strongly on how the CPD was considered (see Crida et al. 2009). As this is the region where both accretion and feedback act directly, our present numerical set up is simply not adequate to address this issue and we defer it to a follow-up work.

7 SUMMARY

The accretion on to giant planets and their associated luminosity can produce observational signatures that reveal the process of planet formation. In this work we used 2D hydrodynamical simulations to study how the accretion and luminosity of a gas giant affects the circumplanetary disc, and the surrounding gap. We extended the procedure used in Montesinos et al. (2015) by taking into account the accretion on to the planet, and computing the planet luminosity accordingly. We have shown that planet accretion feedback does not prevent the development of detectable accretion rates.

Our simulations show that while the planetary feedback is able to partially deplete the circumplanetary disc and reduce its accretion rate, the drop in accretion and luminosity is less than 50%. At this point the planet still has luminosities above $10^{-4} - 10^{-3}L_{\odot}$, that can produce detectable signatures. We note that this occurs even if only a 10% of the planet luminosity is absorbed by the surrounding gas, which is quite plausible since previous studies show that the CPD remains both geometrically and optically thick. The CPD temperature is also increased by the planet luminosity, and can produce a signal of between 5–15 mJy at 20–25 μm . This flux is due to both the inner accretion disc nearby the planet, and the gas heated up further out. The fraction coming from either component depends on the feedback efficiency factor considered in our models.

The feedback effects are not limited to the CPD – the gap carved by the planet is partially refilled due to the coupling between the planet luminosity and accretion, and to a lesser extent due to the increase in the gap temperature and viscous torque. Finally, the orbital velocity of the gap becomes more Keplerian due to the change in the pressure gradient, and vortex structures are formed near the planet and transported towards the gap when the planet feedback is turned on. These effects may influence the dust transport and evolution, by changing the rate of concentration of particles at the dust traps.

To conclude, understanding planet accretion feedback is both important to correctly interpret the accretion signatures of proto-planet candidates, and to properly model the hydrodynamics of discs, especially in the CPD and gap regions.

ACKNOWLEDGMENTS

We would like to thank P. Benítez-Llambay, W. Lyra, H. Klahr, C.P. Dullemond, N. Cuello, S. Stammer, D. Stamatellos, S. Casassus, and J.A. Eisner for their comments, suggestions and helpful discussions that greatly improved the quality of this work. This work was partly carried out while JC was on sabbatical leave at MPE. JC and MG acknowledge the kind hospitality of MPE, and funding from the Max Planck Society through a “Partner Group” grant. We acknowledge financial support from Millennium Nucleus grant RC130007 (Chilean Ministry of Economy), from CONICYT-Chile through FONDECYT (1141175, JC & MG; 1150345, MG), CONICYT-Gemini (32120007, MM) and Basal (PFB0609, JC & MG) grants, and from the European Research Council (ERC) under the European Union’s

Horizon 2020 research and innovation programme (grant agreement No 714769, MG).

REFERENCES

- Ayliffe, B. A., & Bate, M. R. 2009, *MNRAS*, 393, 49
 Ayliffe, B. A., & Bate, M. R. 2009, *MNRAS*, 397, 657
 Baruteau, C., & Masset, F. 2008, *ApJ*, 678, 483
 Benítez-Llambay, P., Masset, F., Koenigsberger, G., & Szulágyi, J. 2015, *Nature*, 520, 63
 Boss, A. P. 1997, *Science*, 276, 1836
 Bryden, G., Chen, X., Lin, D. N. C., Nelson, R. P., & Papaloizou, J. C. B. 1999, *ApJ*, 514, 344
 Cieza, L., Padgett, D. L., Stapelfeldt, K. R., Augereau, J., Harvey, P., Evans, N. J., II, Mern, B., Koerner, D., Sargent, A., van Dishoeck, E. F., Allen, L., Blake, G., Brooke, T., Chapman, N., Huard, T., Lai, S., Mundy, L., Myers, P. C., Spiesman, W., & Wahhaj, Z. 2007, *ApJ*, 667, 308
 Commerçon, B., Teyssier, R., Audit, E., Hennebelle, P., & Chabrier, G. 2011, *A&A*, 529, A35
 Crida, A., Baruteau, C., Kley, W., & Masset, F. 2009, *A&A*, 502, 679
 D’Angelo, G., Kley, W., & Henning, T. 2003, *ApJ*, 599, 548
 Dipierro, G., Laibe, G., Price, D. J., & Lodato, G. 2016, *MNRAS*, 459, L1
 Dong, R., Zhu, Z., Rafikov, R. R., & Stone, J. M. 2015, *ApJL*, 809, L5
 Dong, R., Zhu, Z., & Whitney, B. 2015, *ApJ*, 809, 93
 Dunhill, A. C. 2015, *MNRAS*, 448, L67
 Dürmann, C., & Kley, W. 2015, *A&A*, 574, A52
 Dürmann, C., & Kley, W. 2017, *A&A*, 598, A80
 Eisner, J. A. 2015, *ApJL*, 803, L4
 Fouchet, L., Maddison, S. T., Gonzalez, J.-F., & Murray, J. R. 2007, *A&A*, 474, 1037
 Frank, J., King, A., & Raine, D. J. 2002, *Accretion Power in Astrophysics*, by Juhan Frank and Andrew King and Derek Raine, pp. 398. ISBN 0521620538. Cambridge, UK: Cambridge University Press, February 2002., 398
 Glasse, A., Rieke, G. H., Bauwens, E., García-Marín, M., Ressler, M. E., Rost, S., Tikkanen, T. V., Vandenbussche, B., & Wright, G. S. 2015, *PASP*, 127, 686
 Helled, R., Bodenheimer, P., Podolak, M., et al. 2014, *Protostars and Planets VI*, 643
 Hubeny, I. 1990, *ApJ*, 351, 632
 Kanagawa K. D., Muto T., Tanaka H., Tanigawa T., Takeuchi T., Tsukagoshi T., & Momose M. 2015, *ApJL*, 806, L15
 Kataoka, A., Muto, T., Momose, M., Tsukagoshi, T., Fukagawa, M., Shibai, H., Hanawa, T., Murakawa, K., & Dullemond, C.P. 2015, *ApJ*, 809, 78
 Klahr, H., & Kley W. 2006, *A&A*, 445, 747
 Kley W. 1999, *MNRAS*, 303, 696
 Lin, D. N. C., & Papaloizou, J. C. B. 1993, *Protostars and Planets III*, eds. E. H. Levy, & J. I. Lunine (University of Arizona Press), 749
 Masset, F. 2000, *A&AS*, 141, 165
 Mercer, A., & Stamatellos, D. 2017, *MNRAS*, 465, 2
 Montesinos, M., Cuadra, J., Perez, S., Baruteau, C., & Casassus, S. 2015, *ApJ*, 806, 253
 Nayakshin, S., Cuadra, J., & Springel, V. 2007, *MNRAS*, 379, 21
 Nayakshin, S., & Cha, S.-H. 2013, *MNRAS*, 435, 2099
 Nayakshin, S. 2015, *MNRAS*, 454, 64
 Owen, J. E. 2014, *ApJ*, 789, 59
 Perez, S., Dunhill, A., Casassus, S., Roman, P., Szulgyi, J., Flores, C., Marino, S., & Montesinos, M. 2015, *ApJL*, 811, L5
 Pinilla, P., Birnstiel, T., Ricci, L., Dullemond, C. P., Uribe, A. L., Testi, L., & Natta, A. 2012, *A&A*, 538, A114
 Quanz, S. P., Amara, A., Meyer, M. R., Kenworthy, M. A., Kasper, M., & Girard, J. H. 2013, *ApJ*, 766, L1
 Pollack, J. B., Hubickyj, O., Bodenheimer, P., Lissauer, J. J., Podolak, M., & Greenzweig, Y. 1996, *Icarus*, 124, 62
 Raettig, N., Klahr, H., & Lyra, W. 2015, *ApJ*, 804, 35
 Rice, W. K. M., Armitage, P. J., Wood, K., & Lodato, G. 2006, *MNRAS*, 373, 1619
 Rieke, G. H., Wright, G. S., Böker, T., Bouwman, J., Colina, L., Glasse, A., Gordon, K. D., Greene, T. P., Güdel, M., Henning, T., Justtanont, K., Lagage, P.-O., Meixner, M. E., Nørgaard-Nielsen, H.-U., Ray, T. P., Ressler, M. E., van Dishoeck, E. F., Waelkens, C. 2015, *PASP*, 127, 584
 Rivier, G., Crida, A., Morbidelli, A., & Brouet, Y. 2012, *A&A*, 548, A116
 Sallum, S., Follette, K. B., Eisner, J. A., Close, L. M., Hinz, P., Kratter, K., Males, J., Skemer, A., Macintosh, B., Tuthill, P., Bailey, V., Defrère, D., Morzinski, K., Rodrigues, T., Spalding, E., Vaz, A., & Weinberger, A. J. 2015, *Nature*, 527, 342
 Shakura, N. I., & Sunyaev, R. A. 1973, *A&A*, 24, 337
 Stamatellos, D. 2015, *ApJ*, 810, L11
 Stone, J. M., & Norman, M. L. 1992, *ApJS*, 80, 753
 Szulágyi, J., Morbidelli, A., Crida, A., & Masset, F. 2014, *ApJ*, 782, 65
 Szulágyi, J., Masset, F., Lega, E., Crida, A., Morbidelli, A., & Guillot, T. 2016, *MNRAS*, 460, 2853
 Szulgyi, J., Mayer, L., & Quinn, T. 2017, *MNRAS*, 464, 3158
 Szulgyi, J. 2017, *ApJ*, 842, 103
 Weidenschilling, S. J. 1977, *MNRAS*, 180, 57
 Zhu Z. 2015, *ApJ*, 799, 16

This paper has been typeset from a \TeX / \LaTeX file prepared by the author.